Journal of Mechanical Engineering Research and Developments
ISSN: 1024-1752
CODEN: JERDFO
Vol. 44, No. 4, pp. 221-232
Published Year 2021

Fatigue Life of Welded Joint Improvement with Various Welding Principles and Shot Peening process for AISI 1020 Low Carbon Steel

Khairia Salman Hassan[†], Sameer K. Fayyadh[‡], Abdullah Dhayea A[† *]

[†] Middle Technical University (MTU) / Institute of Technology-Baghdad- Department of Mechanic Technician.
[‡] Agriculture college, University of Baghdad, Abu-ghraib, Baghdad – Iraq.

*Corresponding Author Email: drabdullah_Dhayea@yahoo.com

ABSTRACT

Many sheets of low carbon steel AISI 1020 were fitted with dimensions (160x120 x 10 mm) are used in this study. Before welding, some of them are subject to shot peening by steel ball to demonstrate the relationship between pre-shot peening and improvement of mechanical properties. The prepared plates shot and shot less, are welded using Gas Tungsten Arc welding with increasing welding current. Welding joint without faults is chosen for the creation of test specimens. Tensile tests are conducted to measure the state of the fatigue loading. Rotating Bending fatigue, residual stresses, microstructure, and micro-hardness tests were performed. The test results show that the DC current of the welding process and shot peening process improves the mechanical properties of the weld joint by20 %and 21% respectively relative to the base metal. In addition, the fatigue life of welded specimens also increased as a result of the microstructure change and the comparative residual stress created by shot peening.

KEYWORDS

low carbon steel, TIG Welding Process, Shot Peening, Fatigue Strength, Residual stress

INTRODUCTION

Low-carbon steels are commonly used in welded steel structures and are disposed depending on the uses to different fatigue conditions. For applied use, Low-carbon steels are readily joined with several common fusion welding processes such as gas tungsten arc welding (GTAW), is an arc welding process that was implemented using a non-exhaustive tungsten electrode to create the arc .The temperature of the electric arc is about 5000 ° C [1, 2]. An inert shielding gas (argon or helium) protects the weld area from air pollution, Heat input influences on the metallurgical structure of the heat affected zone (HAZ), weld zone. In addition, heat input was also contributed for determining the width and size of the HAZ area. steel parts are present residual stresses and various microstructures that can result in close by lower mechanical properties related to the base material. For instance, weld fatigue life is shorter than that of the base material due to welding defects or softening heat-affected zone (HAZ) [3,4] where fatigue fracture happens in these areas. Fatigue is a failure mechanism where the system fails when it gets a repeated cyclic stress after a period of time in operation. Failure will occur even if this stress is significantly below the metal yield strength as the other factor in causing failure is the number of stress cycles experienced by the component. Failure often happens normal to the main stress practical and the surface of the fracture is distinguished by the supposed 'beach marking' where variations in the stress level offer different rates of crack propagation. The fatigue strength of low carbon steels with low yield stress observed is similar as associated to fatigue strength of welded structural amounts. The probable explanation for this is that the stress concentration and welding defects close to the weld toe contribute to a short initiation time of fatigue crack, HAZ's fatigue strength is greater than that of base metal .This was associated with the microstructure form and hence the corresponding tensile strength [1]. Many researchers have found that the fatigue crack starts at the welding edge due to the concentration of stress that increased the effect of force by the existence of micro crack-as faults at the welded edges. The residual stress on tensile also decreases fatigue life . A variety of methods are being developed for improving the fatigue life of welded joints one of this method is shot peening,

which is typically used to form a film of residual compressive stress on the surface. In this method the surface of the work piece is bombarded with small spherical glass, ceramic or metallic projectiles that form a plastic deformation film .The fatigue strength of the base metals and welded joints is achieved by residual stresses which are increased by residual compressive stresses and decreased by means of residual tensile stresses[5,6]. In general, a welded joint has some single features that make some parameters far more important than others. Fatigue life can be determined by using S-N curves, which draw depending on the results come from fatigue testing[7]. Basquins equation is one of the empirical equations used to approximate results, and is described as: [8]

$$\sigma_f = A(N_f)^{\alpha} \quad (1)$$

Where:

σ_f , reversed stress. N_f , the number of cycles to failure. A and α are material constants. In low carbon steel which , the microstructure in the weld zones and base metal includes ferrite and pearlite particles, and high hardness is found in the region of weld metal and HAZ, indicating its value. Recently, researchers have good attention about improving fatigue life of welded joint [9]. The present study examined fatigue behavior and life improvement of the low carbon steel 1020 AISI weld joint. Fatigue life improvement was achieved by pre-shot of the welded plate and base plate in parallel with the use of different welding parameters which is DC current at each step. This can also redistribute the tension concentration, as the grain shape shifts.

Experimental work

Marital used

Low carbon steel 1020 AISI which used in many steel components such as bridges, building structure, shafts) is select. Chemical analysis was done by (Thermo ARL 3460, optical Emission spectrometer). The obtained results, which is similar to the American standard, are listed in Table 1. Table 2. show selected mechanical properties of 1020AISI.

Table 1. Chemical composition of the low carbon steel 1020 AISI.

Wt% of element	C	Si	Mn	Cr	Mo	Cu	Co
Actual value %	0.2	0.009	0.65	0.011	0.004	0.041	0.004
Standard value %	0.18-0.23	0.01	0.3-0.6	-	-	-	-
Wt% of element	V	W	Ai	Ni	P	S	
Actual value %	0.0009	0.003	0.001	0.012	0.09	0.05	
Standard value %	-	-	-	-	0.04	0.05	

Table 2. Standard Mechanical properties of 1020 AISI

Properties	**Value**
Density (1000 Kg/m^3)	7.7-8.03
Poison's ratio	0.27-0.3
Elastic Modulus (Gpa)	190-210
Tensile strength (Mpa)	394.7
Yield strength (Mpa)	294.8
Elongation (%)	36.5
Hardness (HB)	111
Impact strength (J) (Izod)	123.4

Dimensional sheets (160 x 120x10 mm) are prepared and cleaned from oxidation and equipped from one edge with V single angle of 45° . Some of these sheets were shot by machine style STB-OB with a diameter of 1.25 mm ball steel and a hardness of 55 HRC. The unit rotates at speed 40 rev / min, the shot time is 30 minutes and the shot angle is 10^{o}. The distance from the machine nozzle to metal surface is 120 mm. Shot peening produced comparative residual stresses which was measured by computerized Lab XRD-6000 shiatsu X-RAY diffraction meter. The strain values were determined and then substituted in Brag law to determine the compressive residual stress which is come to be (-241MP) from device. It is obvious from the SAM photo figure (1A) that the plastic deformation was formed on the specimen surface as a result of shot peening process. Also, Figure (1 B) show the Photo graph of the plate subjected to shot peeing before welding.

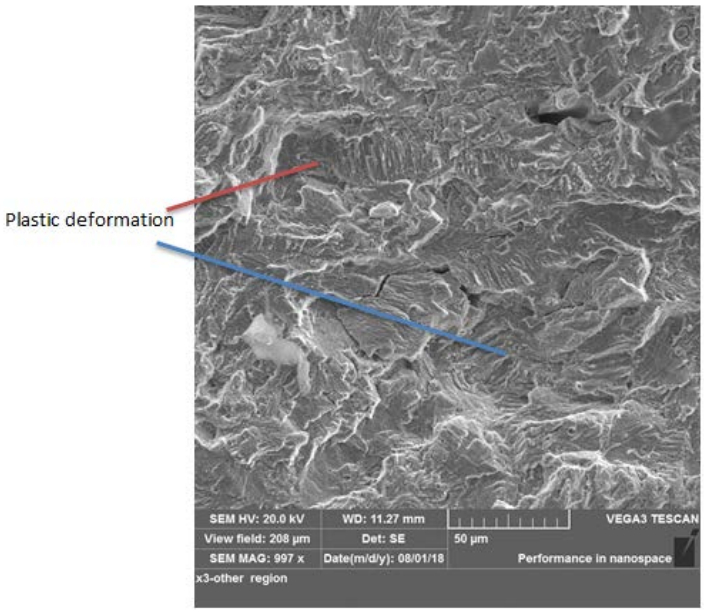

(a)

(b)

Figure 1. (a) ASM photo graph for plats peening surface; (b) Photo graph of the plate subjected to shot peeing before welding.

The prepared sheets are reserved in location with respect to each other and welding is performed by TIG manual welding process with conditions listed in Table (3). As current is varied in four passes, the voltages and welding speed are fixed. The filler metal ER70S-3 with (2.5mm diameter) and chemicals analysis listed in Table (4) is used and the amount of argon inert gas was 10 $\frac{l}{min}$. Heat input rate (arc energy in$\frac{J}{mm}$) was given by the following relation [10].

Heat input = V×I× $\frac{60}{v}$ (2)

Where, V is arc voltage in volts, I is welding current in ampere, v is speed of welding in $\frac{mm}{min}$.

The various weld joints for each state are shown in Figure (2A, B) have symbols (B,C,D,E,F)
Symbol (A) also reveals to the base without welding and the Specimens are fitted with base and weld joints for all examinations.

Table 3. The conditions of the (TIG) welding procedure.

Specimens Symbol	**Number of passes**	**Current (Amp) for each pass.**				**Voltage Volt**	**Heat Input $\frac{J}{mm}$**
		1	2	3	4		
B	4	270	200	175	150	20	1988
C	4	270	200	175	150	=	1988
D	4	250	200	190	180	=	1892
E	4	250	200	190	180	=	1892
F	4	280	240	230	200	=	2192

Table 4. The chemical analysis of wire filler ER70S-3.

Element wt%	**C**	**Si**	**Mn**	**S**	**Ni**	**Cr**	**Cu**	**P**
Stander	0.06-0.15	0.45-0.75	0.9-1.4	0.02	0.15	0.025	0. 5	0.025max.
Real value	0,07	0.52	1.19	0.022	-	-	0.4	0.012

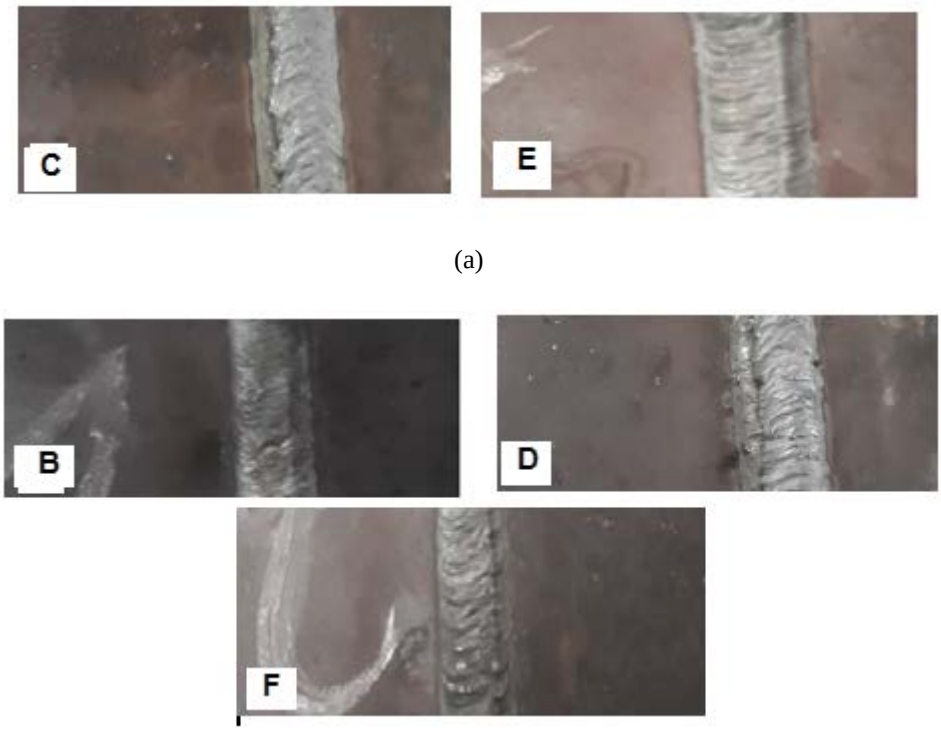

(a)

(b)

Figure 2. (a) Image of the weld joints subjected to shot peening before welding; (b) Image of the weld Joints without shot peening.

A variety of procedures such as grinding, polishing and etching by Nital solution for 20 seconds were performed before the tests to analyze the microstructure using the optical microscope supplied with the camera. The microstructure of all specimens has been observed in figure (3).

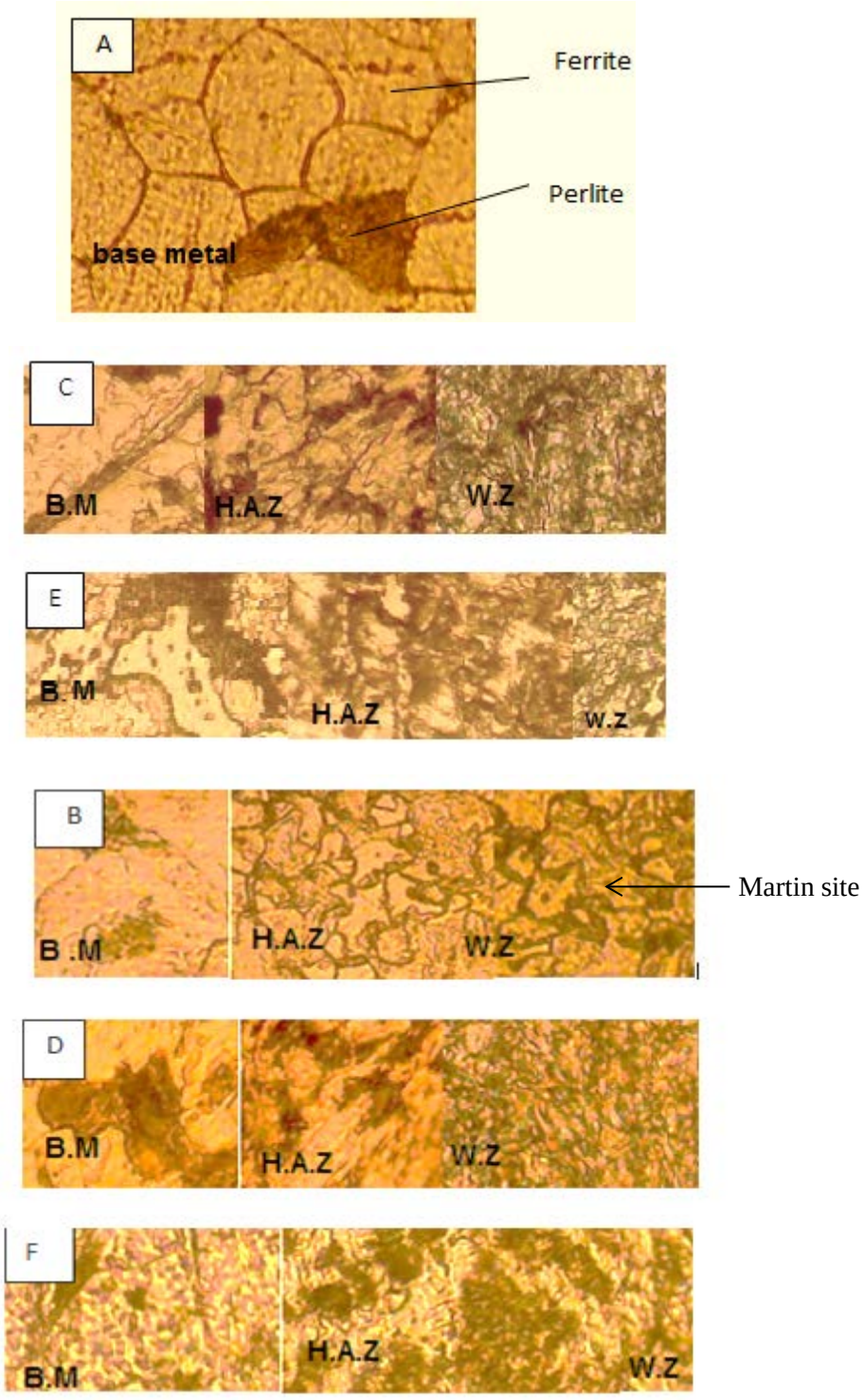

Figure 3. Microstrucher of all weld joint and base metal at(40x)

Surface roughness

The points determined in the entire sample outer region are the sum of three measurements of free surface roughness. The centralize-line mediocre of effects in line peaks is shown in table (4) using the factor Ra that is shown.

Table 4. The results of surface roughness.

Specimen Symbol	A	B	C	D	E	F
Surface roughness Ra (µm)	0.095	0.034	0.085	0.055	0.082	0.095

Micro Hardness test

For hardness sketch across the TIG weld joint and the implications in Figure (4). It clearly shows a dome shape that shows that in the weld zone the hardness is high compared to that of the other zones.

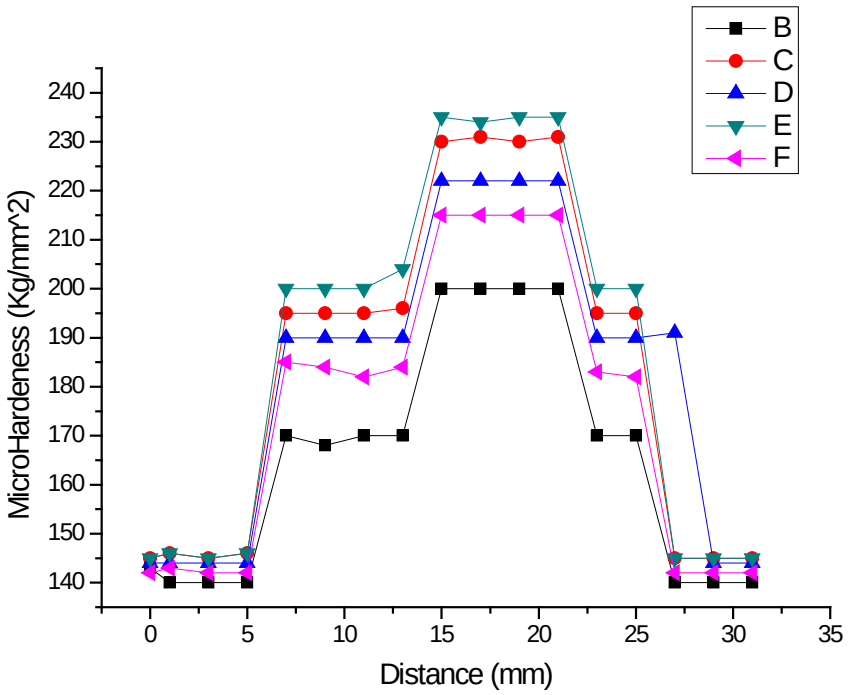

Figure 4. The Vickers hardness profiles of a transverse cross section welds zone.

Tensile Examination

In order to define the mechanical properties of materials, such as strength and ductility, tensile testing is applied. For samples fitted in the measurements shown in Fig. (5A) and Fig. (5B) agreeing to ASTM176000, The tests were done using device smart series with preload assessment 100 kN and 20 (mm/min) cross head speed for all samples in Table (2). The average values for three sample for each test are in Table (5) and Figure (6A,B)

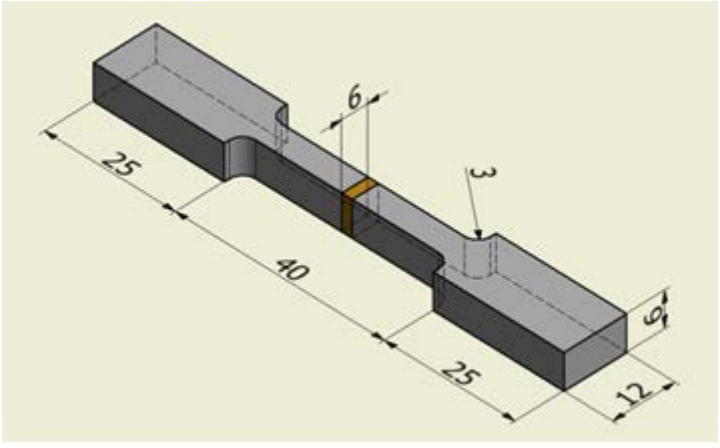

(a)

(b)

Figure 5. (a) Tensile test specimens' measurements (mm); (b) Image of tensile test specimens

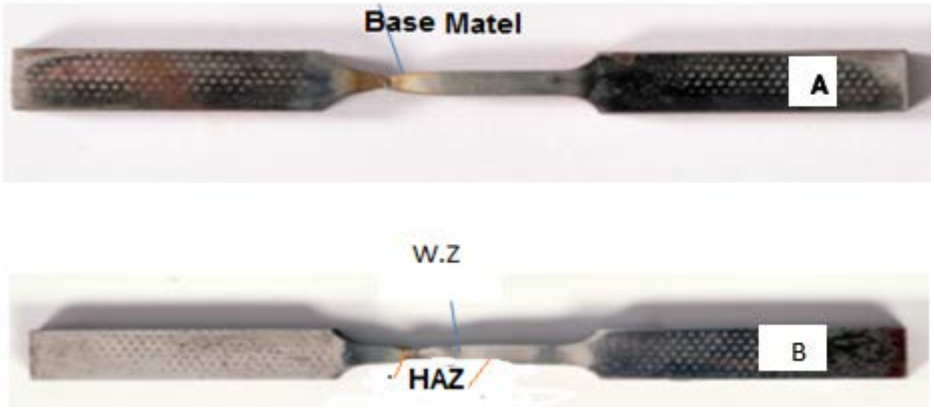

Figure 6. Image of tensile specimens after test

Table 5. The average of true tensile test result for all specimens.

Specimens Symbol	σ_Y Mpa	σ_u Mpa	σ_F Mpa	ε
A	290	400	280	30
B	365	477	377	22
C	380	480	390	19
D	365	476	370	21
E	390	485	397	23
F	336	481	340	22

Figure (7) shows the relation between stress and strain for all tensile test specimens . It is apparent that all specimens display greater stress than the sample of the specimens A metal base. This action can be due to the change that occurs in welding microstructures. In addition, all test specimens show a greater welding period, which will take longer to fail. Samples that have high stress and strain values are said to be tough, and tough materials are normally suitable for design use.

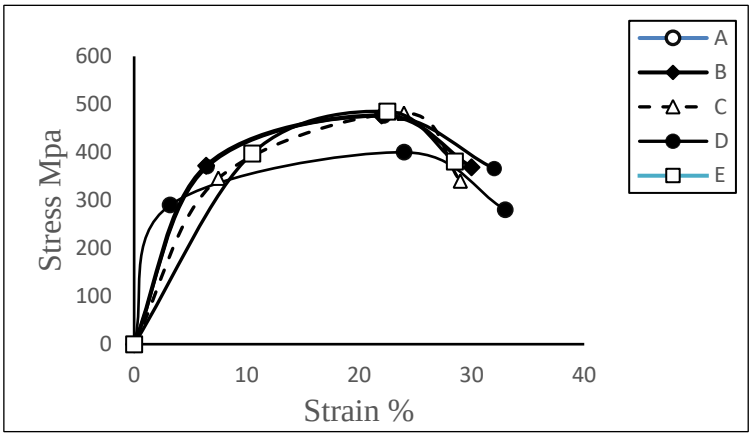

Figure 7. Stress-strain curve for all specimens.

Fatigue Test

Low carbon steel AISI 1020 fatigue samples of base and TIG weld joints were machined into the samples using CNC machines as shown in Figure (8A) according to ASTM (E8 / E8M09) specification As shown in Figure (8B), a fatigue-testing system of style (SCHENCK) PUNN rotating bending is chosen to conduct all fatigue tests with constant tension, The sample is exposed to a practical load from the right side of the specimen axis, resulting in a moment of bending. The surface of the specimen is therefore subjected to stress of tension and compression as soon as rotating Figure(8C). The weight (P) is dignified using Newton (N), carried out to the sample to obtain the stress (σ) and can be found from the relation below: [10]

$$\sigma_b = \frac{32\times125.7\ P(N)}{\pi\times d^3} \tag{3}$$

Where: (σ_b) is the practical stress (MPa), (P) is the load, the arm equal to 125.7mm and the total diameter of the sample is (d) (mm). Figure (9A,B) show the fatigue behavior of all specimens weld joint and base metal low carbon steel AISI 1020.

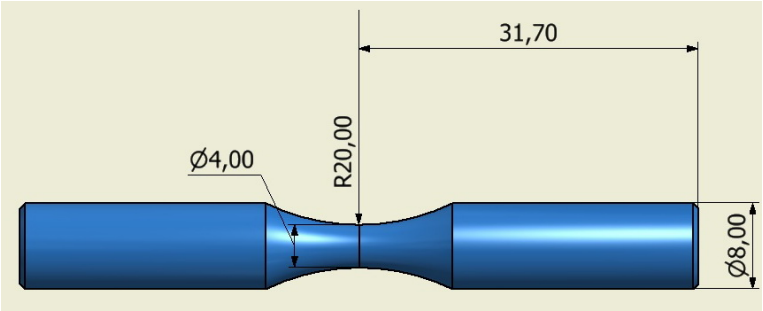

(a)

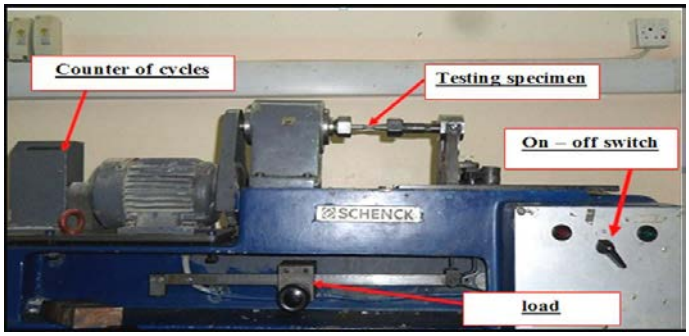

(b)

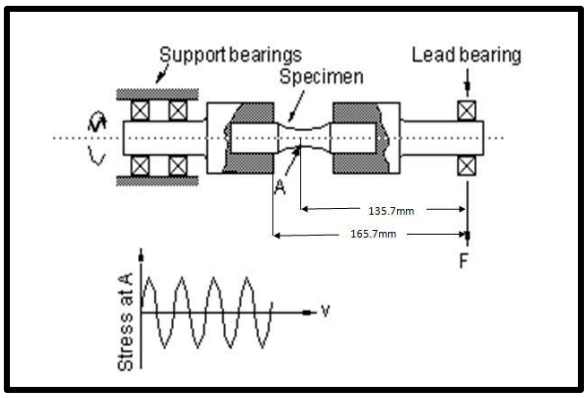

(c)

Figure 8. (a) Fatigue test specimen in mm; (b) SCHENCK PUNN Rotary fatigue bending machine; (c) Application load with the arm.[11]

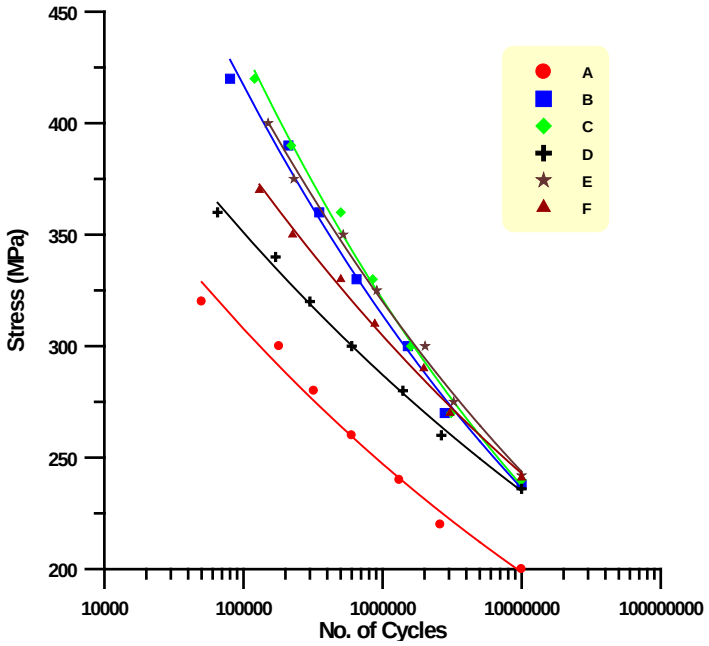

(a)

(b)

Figure 9. (a) S-N curve for all specimens; (b) Image of specimen after test.

The Low Carbon steel at constant stresses for all specimens were clear by the Basquin equation as $\sigma_f = A\ N_f^{-\alpha}$ Where: σ_f : Fatigue limit in Mpa, A: constant, $-\alpha$: the slope of the curve. This equation was implemented to provide the (fatigue limit) at 10^7 cycles. The following equations are fitted to obtain a mathematical representation of the curve Table 6.

Table 6. Fatigue limit and S-N curve equation for all specimens.

Specimens symbols	(Fatigue Limit) at $(10)^7$cycle in MPa	S-N Curve Equations
A	201	$\sigma_f = 901.44578\ N_f^{-0.093556852}$
B	230	$\sigma_f = 1697.2411\ N_f^{-0.12211464}$
C	240	$\sigma_f = 1942.4729\ N_f^{-0.13030386}$
D	242	$\sigma_f = 951.1215\ N_f^{-0.086672029}$
E	244	$\sigma_f = 1612.3497\ N_f^{-0.11703103}$
F	241	$\sigma_f = 1168.4244\ N_f^{-0.097262933}$

The crack propagation for specimen (A) was shown in figure (10). The crack started in the ferrite grain region and propagates until it reached to perlite region. However, it changes its direction to avoid the perlite grain region.

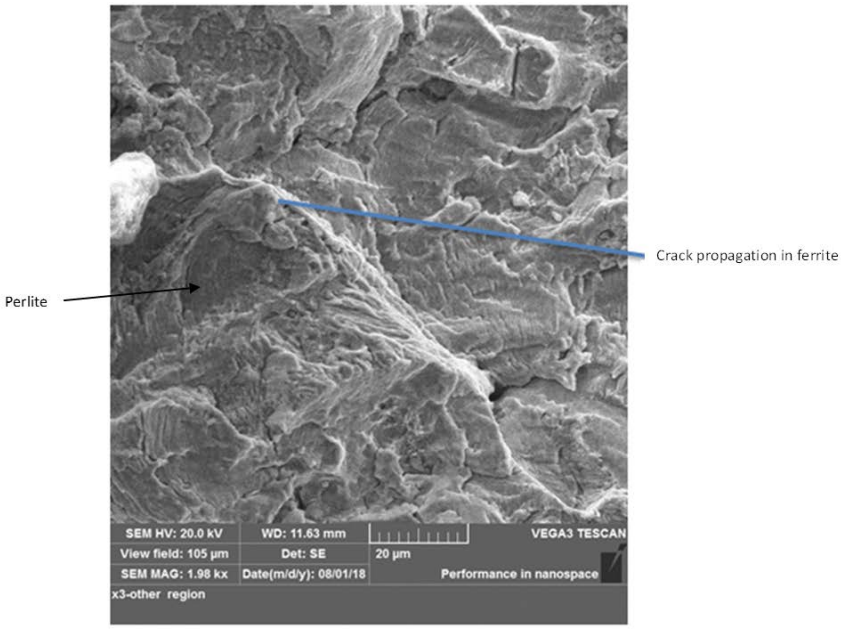

Figure 10. Scan photo graph for fracture of base metal

DISCUSSION

Figure (3A) The low carbon steel 1020 AISI base metal micro structure includes ferrite and pearlite, microstructure of weld joints is shown in Figure (3B, C, D, E, F) also have ferrite and pearlite but the location of pearlite and ferrite is different because of the incomplete diffusion period for carbon under high heating rates in the welding [7]. In addition, by heat input, this can be enhanced to obtain a circular ferrite structure in the weld zone and this is the goal of this paper and the quantity of heat input depends on factors such as current, voltage and wire speed of the heat supply, it is obvious from Figure(3B) that the microstructure becomes finer with the change of current for each pass as seen in TABLE 3. This behavior improves the mechanical properties that differ from one weld joint to another. On the other hand, weld area hardness is greatly higher than base metal.

This can be used to the formation of fine perlite in the weld area.HAZ hardness was start to be lesser than welde d region chiefly due to the formation of ferrite and perlite due to the little cooling rate. Tensile testing data is given in Table (5). The weld joint's tensile strength was found to be higher than base metal. In addition, the value of yield strength relative to the base metal is greater. Figure (9A) shows that the fatigue life of specimens (B, C , D, E, F) has increased. Compared to base metal (A), the changes in the fatigue limit are seen in Table (6), which indicates improvement in the tensile strength. This shift occurred due to the shot peening mechanism that led to the formation of a comparative residual stress layer (C, E) that increases with increasing shot time [16]. This layer delays the crack of fatigue on the surface of specimens. In the ferrite grain, the fatigue crack initiates and propagates rapidly and then ends at the pearlite grain.

Depending on the reference [17], it is clear that this process did not occur when the crack began in the perlite grain. On the other hand, when it started at the ferrite zone, the crack propagates quickly as shown in figure (10), which agreed with the results cited by[17]. The shot peening method was used to increase the potential of the weld to advance the mechanical equality of the welded metal. To increase the welding capacity that encourages the mechanical equality of the welded metal, the shot peening process was used. It is obvious that the shot peening contributes to surface plastic deformation, which leads to an improvement in the hardness of the pressure. All of these variables worked together to increase the lifetime limit of fatigue. In TABLE 6 and Figure (9A,B), the difference in fatigue limit can be seen.

CONCLUSIONS

From the experimental investigation into the behavior of TIG welded joint for low carbon steel AISI 1020 with shot peening, the following results can be found:

1. Microstructures of low carbon steel weld joint were affected by heat input**.** Homogeneous heat input extends the fusion line and that leads to increase in hardness. Additionally, high current refine the grain size in ferrite phase.
2. The welding current affect the HAZ due to the high heat input causing to increase in grain size.
3. The yield and tensile strength increased with the increasing of welding current and compressive residual stress produced by shot peening.
4. Because of the increase in heat input as the weld current increased with each pass, the decrease in strain occurred as a result of high tensile and yield power.

5- Due to the increase in tensile properties by increasing welding current with each pass and with shot peening, the fatigue life for all weld joints has been increased.

6- Shot peening improved the weld joint mechanical equality by around 83 percent compared to base metal.

REFERENCES

[1] W.M. Jodia, "Study the Change of Current Weld on Mechanical Properties and Microstructure of Low Carbon Steel Welded by Electric Arc Welding" *Journal of Babylon University, Engineering Sciences*, No.4, Vol. 25, Pp. 1470-1477, 2017.

[2] R. Sudarshan, and D.R.M. Devaiah, "Effect of Process Parameters in MIG Welding on Mild Steel IS 2062 " *International Journal of Applied Engineering Research*, Vol. 13, No. 4, Pp. 2046-2054, 2018.

[3] W.S.H.W. Muda, N.S.A.M. Nasir, S. Mamat, and S. Jamian, “Effect of Welding Heat Input on Microstructure and Mechanical Properties at Coarse Grain Heat Affected Zone of ABS Grade a Steel", *ARPN Journal of Engineering and Applied Sciences*, Vol. 10, No 20, Pp. 9487-9495, 2015.

[4] Knowledge Article from, “Fatigue of Metals: Part One ",2005. www.Key-to-Steel.com

[5] J. Krebs, and M. Kassner, “Influence of Welding Residual Stresses on Fatigue Design of Welded Joints and Components”, *Welding in the World*, Vol. 51, No 7/8, Pp. 54-63, 2007.

[6] K.E. Hansen A/S,” Aluminium Fatigue Tests”, 2000.

[7] M. Dewan, G. González, and M.A. Wahab, “Effects of Rotating-Bending and Torsional Fatigue Loads on Gas Tungsten Arc (GTA) Welded AISI 1018 Low Carbon Steel Joints", *International Manufacturing Science and Engineering Conference*, Pp.1-7, 2015.

[8] R. Mohammed, D.M. Reddy and G.S. Rao, "Comparative Studies on Microstructure, Mechanical and Corrosion Behavior of DMR 249A Steel and its Welds", *Materials Science and Engineering*, 330, Pp. 1-8, 2018.

[9] Z.D. Perović, “Investigation of the Fatigue Strength of the Welded Joints Treated by TIG Dressing", 12th International Research/Expert Conference "Trends in the Development of Machinery and Associated Technology" TMT 2008, Istanbul, Turkey, Pp. 197-200, 2008.

[10] C. Li, and W. Dai, "Fatigue Life Estimation of Medium-Carbon Steel with Different Surface Roughness", *Applied Sciences*, Vol. 7, No. 338, Pp. 1-11, 2017.

[11] N.S.M. Nasir, M.K.A. Abdul Razab, M.I. Ahmad, and S. Mamat, "Influence of Heat Input on Carbon Steel Microstructure", *ARPN Journal of Engineering and Applied Sciences*, Vol. 12, No. 8, Pp. 2688-2697, 2017.

[12] M.K. Abbass, and K.S. Hassan, "Influence of the Butt Joint Design of TIG Welding on Corrosion Resistance of Low Carbon Steel", *American Journal of Scientific and Industrial Research*, Vol. 3, No. 1., Pp. 47-55, 2012.

[14] S. Benchouia, N. Merakrb, S. Adjel, S. Ehlers, M. Baccouche, and A. Kaddour”, Fatigue Life Enhancement of TIG-Welded 304L Stainless Steel”, *The International Journal of Advanced Manufacturing Technology*, 2018.

[15] A.M. Witteck, D. Gaska, B. Lazarz, and T. Matyja, “Effect of Shot Peening of the Fatigue Strength of Automotive Tubular Stabilizer Bars DC218”, *Archives of Metallurgy and Materials*, Vol. 61, No.4, Pp. 1963-1968, 2016.

[16] N.A. Saad, A.H. Hashim, and G.A. Kadum, “Effect of Shot Peening Time on Mechanical Properties of Aluminum Alloy AL2024 –T4”, *The Iraqi Journal for Mechanical and Material Engineering*, Vol. 14, No.1, 2014.

[17] M. S. Waheed, "The Effect of Some Surface Treatments of Carbon Steel on Fatigue Behavior ", Phd Thesis in Applied Physics, Department of Applied Science, University of Technology, 1995.